

Femtosecond reduction of atomic scattering factors triggered by intense x-ray pulse

Ichiro Inoue^{1,*}, Jumpei Yamada², Konrad J. Kapcia^{3,4}, Michal Stransky^{5,6}, Victor Tkachenko⁴,
Zoltan Jurek⁴, Takato Inoue⁷, Taito Osaka¹, Yuichi Inubushi^{1,8}, Atsuki Ito², Yuto Tanaka²,
Satoshi Matsuyama^{2,7}, Kazuto Yamauchi^{2,9}, Makina Yabashi^{1,8}, and Beata Ziaja^{4,6†}

¹RIKEN SPring-8 Center, 1-1-1 Kouto, Sayo, Hyogo 679-5148, Japan.

²Department of Precision Science and Technology, Graduate School of Engineering,
Osaka University, 2-1 Yamada-oka, Suita, Osaka 565-0871, Japan

³Institute of Spintronics and Quantum Information,
Faculty of Physics, Adam Mickiewicz University in Poznań,
Uniwersytetu Poznańskiego 2, PL-61614 Poznań, Poland.

⁴Center of Free-Electron Laser Science CFEL, Deutsches
Elektronen-Synchrotron DESY, Notkestr. 85, 22607 Hamburg, Germany.

⁵European XFEL GmbH, Holzkoppel 4, 22869 Schenefeld, Germany.

⁶Institute of Nuclear Physics, Polish Academy of Sciences, Radzikowskiego 152, 31-342 Krakow, Poland.

⁷Department of Materials Physics, Graduate School of Engineering,
Nagoya University, Furo-cho, Chikusa, Nagoya, 464-8603, Japan.

⁸Japan Synchrotron Radiation Research Institute, Kouto 1-1-1, Sayo, Hyogo 679-5198, Japan.

⁹Center for Ultra-Precision Science and Technology,
Graduate School of Engineering, Osaka University,
2-1 Yamada-oka, Suita, Osaka 565-0871, Japan.

X-ray diffraction of silicon irradiated with tightly focused femtosecond x-ray pulses (photon energy: 11.5 keV, pulse duration: 6 fs) was measured at various x-ray intensities up to 4.6×10^{19} W/cm². The measurement reveals that the diffraction intensity is highly suppressed when the x-ray intensity reaches of the order of 10¹⁹ W/cm². With a dedicated simulation, we confirm the observed reduction of the diffraction intensity is attributed to the femtosecond change in individual atomic scattering factors due to the ultrafast creation of highly ionized atoms through photoionization, Auger decay, and subsequent collisional ionization. We anticipate that this ultrafast reduction of atomic scattering factor will be a basis for new x-ray nonlinear techniques, such as pulse shortening and contrast variation x-ray scattering.

Knowledge of the structure of matter at atomic resolution is critical for understanding and accurately predicting material properties. Since its discovery at the beginning of the twentieth century, x-ray scattering has been a primary tool for atomic-scale structural studies of various systems in physical, chemical, and biological sciences [1].

The recent advent of x-ray free-electron lasers (XFELs) [2, 3], which produce femtosecond hard x-ray pulses, is enhancing the capabilities of x-rays as an atomic-resolution probe. When an XFEL pulse irradiates matter, photo-, Auger, and collisionally excited electrons are emitted during or soon after the x-ray exposure [4–7]. Although such electron excitations can trigger subsequent atomic disordering through the electron-lattice interaction and the modifications of interatomic potential [8–10], it has been predicted [11] and experimentally confirmed [12–14] that there is a several femtosecond time delay between the x-ray exposure and atomic displacements. Therefore, the ultrafast XFEL pulses allow the measurement of diffraction signal before the onset of the atomic displacements and mitigate radiation damage in the samples, which has been a long-standing bottleneck for x-ray structure determination [15–18].

Based on this diffraction-before-destruction concept [19], a large number of structures of protein microcrystals have been solved using XFEL pulses [20, 21]. In these experiments, the XFEL pulses were focused to a few micrometer spot size to increase the number of photons irradiating the sample. Even though the intensity and fluence of the microfocused XFEL pulses reached as high as the order of 10¹⁷ W/cm² and 10³ J/cm², respectively, no significant electron density gain and loss were observed in the electron density map of the determined structures [22], indicating that the incident photons were predominately scattered by pristine atoms that had neither been photoionized nor collisionally ionized.

Recent developments in nanofocusing optics for XFEL pulses [23–28] will further strengthen the capabilities of x-ray structure determination. The high intensity and fluence of the nanofocused pulses (more than 10¹⁹ W/cm² and 10⁵ J/cm², respectively) will reduce the required crystal sizes for structure determination and thereby largely expand the targets of x-ray crystallography. However, numerical simulations predict that the majority of the atoms are ionized during the x-ray exposure [19, 29, 30] and that the atomic scattering factors become lower than those for neutral atoms [31, 32]. Thus, it is not appropriate to use conventional procedures for the structure analysis, and one needs to develop new methodologies that incorporate the ultrafast

* inoue@spring8.or.jp

† beata.ziaja-motyka@cfel.de

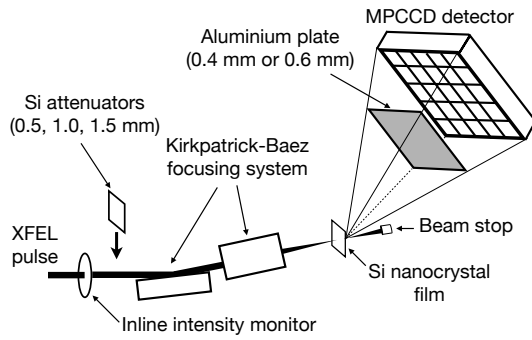


FIG. 1. A schematic illustration of the experiment.

changes in the atomic scattering factors [33]. On the positive side, the measurement at different x-ray intensities enables contrast variation of scattering strengths for different atomic constituents [34, 35], which is highly useful for phasing. Also, the loss of the x-ray diffraction at high intensity can be a basis for nonlinear x-ray optical devices, particularly those for pulse shaping, as discussed later.

Until now, studies on how materials behave under irradiation with an XFEL pulse with intensities beyond 10^{18} W/cm^2 have mostly relied on theoretical modeling. Although a few pioneering groups experimentally evaluated transient atomic displacements of model systems after irradiation with the nanofocused XFEL pulses (diamond [12, 13], xenon clusters [36], and protein crystals [37]), accurate experimental analysis of the ultrafast reduction of atomic scattering factors at high x-ray intensity has not been performed. There remain fundamental questions, such as whether and how much the atomic scattering factors are suppressed at high x-ray intensity.

We describe here an x-ray diffraction measurement of silicon (Si) under irradiation of femtosecond x-ray pulses for different peak intensities and fluences up to $4.6 \times 10^{19} \text{ W/cm}^2$ and $3.0 \times 10^5 \text{ J/cm}^2$, respectively. By employing the unique capability of SACL A [38] that can generate XFEL pulses with duration well below 10 fs [39–41], we measured the x-ray diffraction signals before the manifestation of the x-ray-induced atomic disordering, which becomes prominent at ~ 20 fs after the x-ray excitation [12–14], and directly evaluated the change in the atomic scattering factors caused by electron excitations. From the comparison between the experimental results and a dedicated simulation, we discuss the detailed mechanism for the ultrafast reduction of atomic scattering factors at high x-ray intensity.

The experiment was performed at experimental hutch 5 of SACL A beamline 3 [42, 43] (Fig. 1). The 11.5-keV x-ray pulses with duration of 6 fs were focused to $180 \text{ nm (horizontal)} \times 150 \text{ nm (vertical)}$ spot by using a Kirkpatrick-Baez focusing system [28]. A $10\text{-}\mu\text{m}$ -thick Si nanocrystal film (grain size of 500 nm, US research nanomaterials) attached to a polyimide film was used as a sample. The sample was placed at the focus, and

five diffraction peaks (111, 220, 311, 400, 331 reflections) in the vertical plane were measured in a shot-by-shot manner with a multiport charge-coupled device detector (MPCCD) [44] that covered the scattering angle (2θ) range of 18° – 53° . To prevent detector saturation, we placed an aluminum plate (thickness of 0.4 mm or 0.6 mm) in front of the detector. The x-ray intensity at the sample position was tuned by inserting or removing Si attenuators with nominal thicknesses of 0.5, 1.0, and 1.5 mm (measured transmittance was 7.52 %, 0.60 %, and 0.045 %, respectively) before the focusing system. The pulse energy at the sample position was monitored by a calibrated inline intensity monitor at the experimental hutch [45], taking into account the transmittance of the Si attenuator. The fluence for each pulse was determined by dividing the pulse energy by the product of horizontal and vertical beam sizes ($180 \text{ nm} \times 150 \text{ nm}$). The peak intensity was calculated by dividing the fluence by $\sqrt{\pi/(4 \log 2)} \cdot \Delta t$ with pulse duration $\Delta t=6 \text{ fs}$.

We compared the diffraction intensities for high and low x-ray intensity conditions as follows. First, we measured 300 successive single-shot diffraction images at the fixed sample position with the 1.5-mm Si attenuator. The x-ray peak intensity and fluence at the sample were $\sim 2.1 \times 10^{16} \text{ W/cm}^2$ and $\sim 1.3 \times 10^2 \text{ J/cm}^2$, respectively, and the x-ray dose was much lower than the predicted damage threshold [9, 46]. From the average diffraction image, we calculated the one-dimensional diffraction intensity profile ($I_{low}(2\theta)$) by azimuthal integration. Next, we reduced the attenuator thickness (0.5 mm or 1.0 mm) or removed the attenuator and measured the single-shot diffraction intensity profile at the same sample position, $I_{high}(2\theta)$. The measurement at low and high x-ray intensities was repeated for different positions. We extracted and analyzed the dataset of $I_{high}(2\theta)$ measured with specific peak intensity $((4.6 \pm 1.2) \times 10^{19} \text{ W/cm}^2$ (without attenuator), $(3.5 \pm 0.9) \times 10^{18} \text{ W/cm}^2$ (Si 0.5 mm attenuator), and $(2.8 \pm 0.7) \times 10^{17} \text{ W/cm}^2$ (Si 1.0 mm attenuator)) and those of $I_{low}(2\theta)$ measured at the same sample positions. For each attenuator condition, the data for ~ 500 different sample positions were extracted. After being normalized by the pulse energy, $I_{high}(2\theta)$ and $I_{low}(2\theta)$ were averaged over different positions. Hereafter, we simply refer to these averaged diffraction intensity profiles as diffraction intensity profiles at high and low peak intensities.

Figures 2 (a)–(c) show diffraction intensity profiles at high peak intensities $((2.8 \pm 0.7) \times 10^{17}$, $(3.5 \pm 0.9) \times 10^{18}$, $(4.6 \pm 1.2) \times 10^{19} \text{ W/cm}^2$) and corresponding diffraction intensity profiles at low peak intensities ($\sim 2.1 \times 10^{16} \text{ W/cm}^2$). Here we placed a 0.4-mm-thick aluminum plate in front of the detector for the measurement shown in Fig. 2 (a), while we selected a 0.6-mm-thick plate for the measurements shown in Figs. 2(b) and 2(c). The background for the diffraction intensity profiles at high and low x-ray intensity conditions was in excellent agreement, indicating that normalization by the pulse energy went well. As

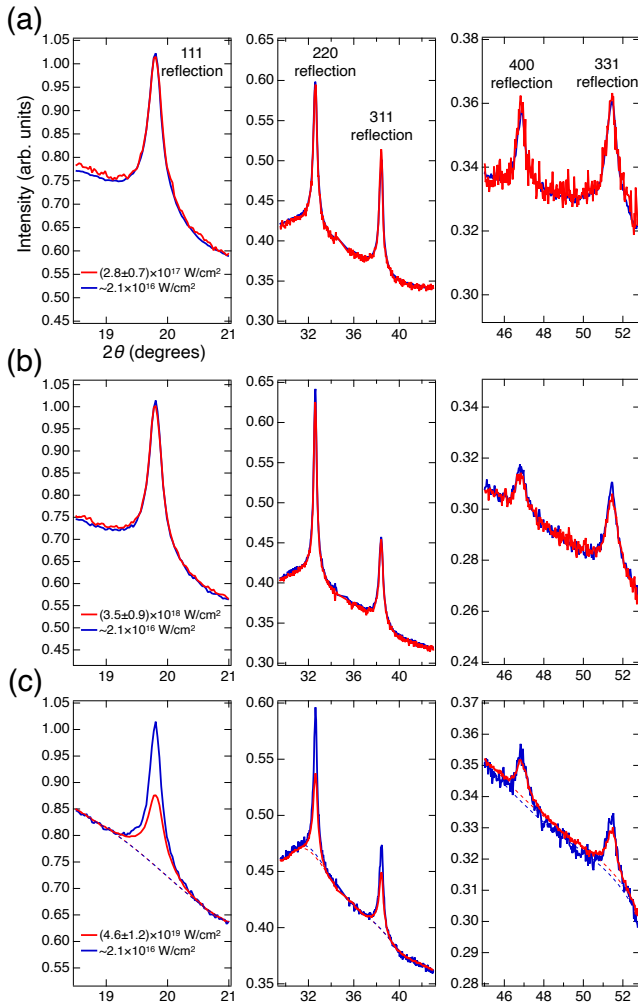


FIG. 2. X-ray diffraction intensity profiles of Si at high peak intensities: (a) $(2.8 \pm 0.7) \times 10^{17} \text{ W/cm}^2$, (b) $(3.5 \pm 0.9) \times 10^{18} \text{ W/cm}^2$, (c) $(4.6 \pm 1.2) \times 10^{19} \text{ W/cm}^2$, and corresponding diffraction intensity profiles at low peak intensity ($\sim 2.1 \times 10^{16} \text{ W/cm}^2$). Dotted curves in (c) represent the estimated background.

seen from Figs. 2(a) and 2(b), the diffraction intensity profiles at the peak intensities of $(2.8 \pm 0.7) \times 10^{17} \text{ W/cm}^2$ and $(3.5 \pm 0.9) \times 10^{18} \text{ W/cm}^2$ are almost the same as that at low x-ray intensity. This result proves that the XFEL pulses with the intensities of up to 10^{18} W/cm^2 do not change the atomic scattering factors and the degree of atomic disordering during the x-ray exposure, validating damage-free protein crystallography using microfocused XFEL pulses (typical intensity and fluence are 10^{17} W/cm^2 and 10^3 J/cm^2 , respectively), which is routinely performed at XFEL facilities [20, 21].

In contrast, the diffraction intensity at the highest peak intensity ($(4.6 \pm 1.2) \times 10^{19} \text{ W/cm}^2$) was suppressed compared with that at low peak intensity (Fig. 2(c)). The observed decrease in the diffraction intensity indicates structural and/or electronic damage in Si crystals during the x-ray exposure. To quantitatively evaluate how much the diffraction intensity was suppressed at high

TABLE I. Ratio of x-ray diffraction intensity of Si normalized by incident pulse energy at high peak intensity ($(4.6 \pm 1.2) \times 10^{19} \text{ W/cm}^2$) to that at low peak intensity ($\sim 2.1 \times 10^{16} \text{ W/cm}^2$).

Reflection (hkl)	$I_{eff}^{hkl} = I_{high}^{hkl}/I_{low}^{hkl}$	$Q (\text{\AA}^{-1})$
111	0.650 ± 0.040	2.00
220	0.735 ± 0.084	3.27
311	0.760 ± 0.138	3.84
400	0.769 ± 0.169	4.64
331	0.724 ± 0.046	5.04

x-ray intensity, we first estimated the background of the diffraction profiles at high and low x-ray intensity by fitting the profiles in the vicinity of diffraction peaks with polynomial functions (dotted curves in Fig. 2(c)). After subtracting the estimated background, each diffraction peak was fitted by a Gaussian function, and the integrated diffraction intensity for hkl reflection ($hkl=111, 220, 311, 400, 331$) was determined (I_{high}^{hkl} and I_{low}^{hkl}). Table 1 summarizes the ratio of the diffraction intensity at high intensity to that at low intensity $I_{eff}^{hkl} = I_{high}^{hkl}/I_{low}^{hkl}$ (hereafter called the diffraction efficiency) and corresponding scattering vector $Q = 4\pi \sin \theta/\lambda$ with the x-ray wavelength λ . The experimental uncertainty of I_{eff}^{hkl} in Table 1 represents the standard deviation of the diffraction efficiency calculated for five independent sub-ensemble datasets. The diffraction efficiency did not depend much on Q , indicating that the atomic disordering during the pulse irradiation (which reduces the diffraction intensity more at higher Q values [47]) was not significant in the present experiment. Thus, it is natural to consider that the observed reduction of the diffraction intensity was attributed to the femtosecond change in atomic scattering factors due to the electronic excitations induced by the XFEL pulse.

To justify this statement, we performed simulations of Si crystal under irradiation with a 6-fs XFEL pulse, using the released version of the molecular dynamics code, *XMDYN* [32, 48, 49]. Neutral atoms, atomic ions, and ionized electrons were treated there as classical particles, and their real-space dynamics were calculated by molecular dynamics technique. The electronic configurations of atoms and ions were followed by taking into account all relevant x-ray-induced processes in matter (such as photoionization, Auger processes, fluorescent decay, and collisional ionization and recombination). Although the focal spot of the XFEL pulses had a Gaussian shape in the present experiment, and the diffraction signals originated from various sample areas with different fluence, we performed the simulations assuming uniform x-ray fluence to reduce the computational cost.

The simulation was performed for the incident pulse with a constant pulse duration (6 fs) and different peak intensities. We found that the simulation results for the

peak intensity of $1.0 \times 10^{20} \text{ W/cm}^2$, could well reproduce the trend of I_{eff}^{hkl} shown in Table 1 (Fig. 3(a)). In Fig. 3(a), the error bars for the simulation results represent the deviation of maximum and minimum values of I_{eff}^{hkl} from the average value obtained from ten independent *XMDYN* simulations. Similarly to the experimental observations, the simulation predicts a nearly constant decrease in the diffraction efficiency for the five reflections ($hkl = 111, 220, 311, 400, 331$). Figure 3(b) shows the simulated root-mean-square atomic displacement during irradiation with the XFEL pulse at the same intensity. For reference, the temporal intensity envelope of the XFEL pulse is also shown. The atomic displacement is much less than lattice spacing for the measured reflections, indicating that the reduction of the diffraction efficiency is not caused by x-ray-induced atomic disordering. Figs. 3(c) and 3(d) show the relative ion population of Si atoms and the average hole numbers in K , L and M -shells per atom. It is clearly seen from Fig. 3(c) that the majority of Si atoms are no more neutral during the x-ray exposure. Furthermore, the x-ray-induced electron excitations are not limited to valence electrons (Fig. 3(d)); many atoms have vacancies in their inner-shells (K and L -shells). Since the atomic scattering factors of neutral and ionized Si atoms are predominantly determined by the spatial distribution of inner-shell electrons, this massive excitation of inner-shell electrons reduces the atomic scattering factor and diffraction efficiency. The simulation results support our hypothesis that the suppression of the diffraction intensity at high x-ray intensity of the order of 10^{19} W/cm^2 , which was observed in the experiment, was caused by the reduction of atomic scattering factors triggered by x-ray-induced electron excitations.

In summary, we measured the x-ray diffraction intensity of Si under irradiation of nanofocused 11.5-keV XFEL pulses. The measurement reveals that diffraction intensity is suppressed at the x-ray intensity on the order of 10^{19} W/cm^2 . From a nearly constant decrease in the diffraction efficiency for the five reflections and a dedicated simulation, we concluded that the reduction of diffraction intensity is attributed to femtosecond change in individual atomic scattering factors due to x-ray-induced electron excitations. We anticipate that the ultrafast reduction of the atomic scattering factors can be a basis for novel applications of high-intensity XFEL pulses. One intriguing application is the nonlinear optical device for pulse shortening in the hard x-ray regime [50]. The simulations results show in Fig. 3 predict that Si crystals under high-intensity x-ray irradiation become highly ionized, and thereby its overall scattering strength is largely suppressed in the second half of the pulse. Therefore, the photons at the leading edge of the pulse are selectively diffracted, effectively making the pulse duration of the diffracted beam shorter than the incident pulse duration. Since the suppression of atomic scattering factors at high x-ray intensity is expected to occur in all materials, thin single crystals made of light

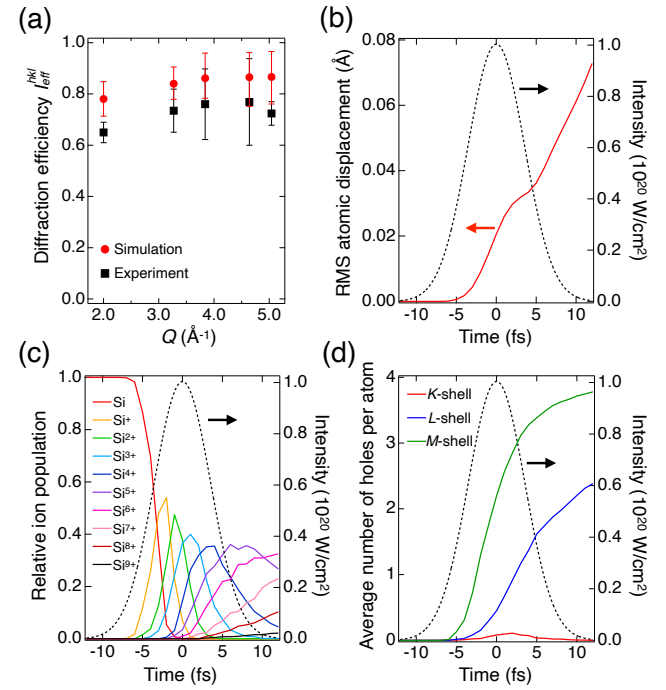


FIG. 3. *XMDYN* simulation results for Si crystal during its exposure to 6-fs XFEL pulse with photon energy of 11.5 keV and peak intensity of $1.0 \times 10^{20} \text{ W/cm}^2$. (a) Comparison of diffraction efficiency for 111, 220, 311, 400, 331 reflections of Si obtained from simulations (red circles) and from experiment (black squares). (b-d) (b) Root-mean-square atomic displacement, (c) relative ion population, and (d) average numbers of K , L , and M -holes per atom, for Si exposed to the XFEL pulse. Time zero corresponds to the intensity maximum of the XFEL pulse. Black dotted curves represent temporal intensity envelope of the XFEL pulse.

elements in Laue geometry are promising candidates for high-throughput optical devices designed to shorten the pulse duration. Such pulse-shorting devices will be essential to perform ultrafast time-resolved experiments at the forthcoming cavity-based XFELs, because the duration of x-ray pulses from these sources will be several tens of femtoseconds or more due to their extremely small bandwidth [51, 52]. Another potential application is the contrast variation x-ray scattering in polyatomic samples. Since the electron-impact ionization cross-sections depend on atomic number [53], we can expect that the magnitude of decrease in the atomic scattering factor at high x-ray intensity will differ from atom to atom. The diffraction measurement at different x-ray intensities will then enable contrast variation of scattering strengths between different types of atoms. This can open a new route for *de novo* structure determination of protein crystals.

We acknowledge Prof. Eiji Nishibori for insightful discussions. The work was supported by the Japan Society for the Promotion of Science (JSPS) KAKENHI Grants (19K20604, 22H03877). K. J. K. thanks the Polish National Agency for Academic Exchange

for funding in the frame of the Bekker programme (PPN/BEK/2020/1/00184). The experiments were performed with the approval of the Japan Synchrotron Radiation Research Institute (JASRI, Proposal Nos. 2021A8057, 2021B8022, 2022A8030).

[1] J. Als-Nielsen and D. McMorrow, *Elements of modern X-ray physics* (John Wiley and Sons, 2011).

[2] E. L. Saldin, E. A. Schneidmiller, and M. V. Yurkov, *The Physics of Free Electron Lasers* (Springer, Berlin, 1999).

[3] B. W. J. McNeil and N. R. Thompson, X-ray free-electron lasers, *Nat. Photonics* **4**, 814 (2010).

[4] B. Ziaja, D. van der Spoel, A. Szöke, and J. Hajdu, Auger-electron cascades in diamond and amorphous carbon, *Phys. Rev. B* **64**, 214104 (2001).

[5] N. Timneanu, C. Caleman, J. Hajdu, and D. van der Spoel, Auger electron cascades in water and ice, *Chem. Phys.* **299**, 277 (2004).

[6] B. Ziaja, R. A. London, and J. Hajdu, Unified model of secondary electron cascades in diamond, *J. Appl. Phys.* **97**, 064905 (2005).

[7] C. Caleman, C. Ortiz, E. Marklund, F. Bultmark, M. Gabrys, F. G. Parak, J. Hajdu, M. Klintenberg, and N. Timneanu, Radiation damage in biological material: Electronic properties and electron impact ionization in urea, *Europhys. Lett.* **85**, 18005 (2009).

[8] N. Medvedev, H. O. Jeschke, and B. Ziaja, Nonthermal graphitization of diamond induced by a femtosecond x-ray laser pulse, *Phys. Rev. B* **88**, 224304 (2013).

[9] N. Medvedev, Z. Li, and B. Ziaja, Thermal and nonthermal melting of silicon under femtosecond x-ray irradiation, *Phys. Rev. B* **91**, 054113 (2015).

[10] N. Medvedev, Z. Fang, C. Xia, and Z. Li, Thermal and nonthermal melting of III-V compound semiconductors, *Phys. Rev. B* **99**, 144101 (2019).

[11] R. Neutze, R. Wouts, D. van der Spoel, E. Weckert, and J. Hajdu, Potential for biomolecular imaging with femtosecond x-ray pulses, *Nature* **406**, 752 (2000).

[12] I. Inoue, Y. Inubushi, T. Sato, K. Tono, T. Katayama, T. Kameshima, K. Ogawa, T. Togashi, S. Owada, Y. Amemiya, T. Tanaka, T. Hara, and M. Yabashi, Observation of femtosecond x-ray interactions with matter using an x-ray–x-ray pump–probe scheme, *Proc. Natl. Acad. Sci. USA* **113**, 1492 (2016).

[13] I. Inoue, Y. Deguchi, B. Ziaja, T. Osaka, M. M. Abdulla, Z. Jurek, N. Medvedev, V. Tkachenko, Y. Inubushi, H. Kasai, K. Tamasaku, T. Hara, E. Nishibori, and M. Yabashi, Atomic-scale visualization of ultrafast bond breaking in x-ray-excited diamond, *Phys. Rev. Lett.* **126**, 117403 (2021).

[14] I. Inoue, V. Tkachenko, K. J. Kapcia, V. Lipp, B. Ziaja, Y. Inubushi, T. Hara, M. Yabashi, and E. Nishibori, Delayed onset and directionality of x-ray-induced atomic displacements observed on subatomic length scales, *Phys. Rev. Lett.* **128**, 223203 (2022).

[15] R. L. Owen, E. Rudiño-Piñera, and E. F. Garman, Experimental determination of the radiation dose limit for cryocooled protein crystals, *Proc. Natl. Acad. Sci. USA* **103**, 4912 (2006).

[16] J. M. Holton, A beginner’s guide to radiation damage, *J. Synchrotron Radiat.* **16**, 133 (2009).

[17] M. R. Howells, T. Beetz, H. N. Chapman, C. Cui, J. M. Holton, C. J. Jacobsen, J. Kirz, E. Lima, S. Marchesini, H. Miao, D. Sayre, D. A. Shapiro, J. C. H. Spence, and D. Starodub, An assessment of the resolution limitation due to radiation-damage in x-ray diffraction microscopy, *J. Electron Spectrosc. Relat. Phenom.* **170**, 4 (2009).

[18] E. F. Garman, Radiation damage in macromolecular crystallography: what is it and why should we care?, *Acta Crystallogr. Sect. D* **66**, 339 (2010).

[19] H. N. Chapman, C. Caleman, and N. Timneanu, Diffraction before destruction, *Phil. Trans. R. Soc. B* **369**, 20130313 (2014).

[20] I. Schlichting, Serial femtosecond crystallography: the first five years, *IUCrJ* **2**, 246 (2015).

[21] T. R. M. Barends, B. Stauch, V. Cherezov, and I. Schlichting, Serial femtosecond crystallography, *Nat. Rev. Methods Primers* **2**, 59 (2022).

[22] S. Boutet, L. Lomb, G. J. Williams, T. R. M. Barends, A. Aquila, R. B. Doak, U. Weierstall, D. P. DePonte, J. Steinbrener, R. L. Shoeman, M. Messerschmidt, A. Barty, T. A. White, S. Kassemeyer, R. A. Kirian, M. M. Seibert, P. A. Montanez, C. Kenney, R. Herbst, P. Hart, J. Pines, G. Haller, S. M. Gruner, H. T. Philipp, M. W. Tate, M. Hromalik, L. J. Koerner, N. van Bakel, J. Morse, W. Ghonsalves, D. Arnlund, M. J. Bogan, C. Caleman, R. Fromme, C. Y. Hampton, M. S. Hunter, L. C. Johansson, G. Katona, C. Kupitz, M. Liang, A. V. Martin, K. Nass, L. Redecke, F. Stellato, N. Timneanu, D. Wang, N. A. Zatsepin, D. Schafer, J. Defever, R. Neutze, P. Fromme, J. C. H. Spence, H. N. Chapman, and I. Schlichting, High-resolution protein structure determination by serial femtosecond crystallography, *Science* **337**, 362 (2012).

[23] C. David, S. Gorelick, S. Rutishauser, J. Krzywinski, J. Vila-Comamala, V. A. Guzenko, O. Bunk, E. Färm, M. Ritala, M. Cammarata, D. M. Fritz, R. Barrett, L. Samoylova, J. Grünert, and H. Sinn, Nanofocusing of hard x-ray free electron laser pulses using diamond based fresnel zone plates, *Sci. Rep.* **1**, 57 (2011).

[24] H. Mimura, H. Yumoto, S. Matsuyama, T. Koyama, K. Tono, Y. Inubushi, T. Togashi, T. Sato, J. Kim, R. Fukui, Y. Sano, M. Yabashi, H. Ohashi, T. Ishikawa, and K. Yamauchi, Generation of 10^{20} W cm $^{-2}$ hard x-ray laser pulses with two-stage reflective focusing system, *Nat. Commun.* **5**, 3539 (2014).

[25] F. Seiboth, A. Schropp, M. Scholz, F. Wittwer, C. Rödel, M. Wünsche, T. Ullsperger, S. Nolte, J. Rahomäki, K. Parfeniuks, S. Giakoumidis, U. Vogt, U. Wagner, C. Rau, U. Boesenberg, J. Garrevoet, G. Falkenberg, E. C. Galtier, H. Ja Lee, B. Nagler, and C. G. Schroer, Perfect x-ray focusing via fitting corrective glasses to aberrated optics, *Nat. Commun.* **8**, 14623 (2017).

[26] S. Matsuyama, T. Inoue, J. Yamada, J. Kim, H. Yumoto, Y. Inubushi, T. Osaka, I. Inoue, T. Koyama, K. Tono, H. Ohashi, M. Yabashi, T. Ishikawa, and K. Yamauchi, Nanofocusing of x-ray free-electron laser using wavefront-corrected multilayer focusing mirrors, *Sci. Rep.* **8**, 17440 (2018).

[27] T. Inoue, S. Matsuyama, J. Yamada, N. Nakamura, T. Osaka, I. Inoue, Y. Inubushi, K. Tono, H. Yumoto, T. Koyama, H. Ohashi, M. Yabashi, T. Ishikawa, and K. Yamauchi, Generation of an X-ray nanobeam of a free-electron laser using reflective optics with speckle interferometry, *J. Synchrotron Radiat.* **27**, 883 (2020).

[28] H. Yumoto, Y. Inubushi, T. Osaka, I. Inoue, T. Koyama,

K. Tono, M. Yabashi, and H. Ohashi, Nanofocusing optics for an x-ray free-electron laser generating an extreme intensity of 100 EW/cm² using total reflection mirrors, *Appl. Sci.* **10** (2020).

[29] S. P. Hau-Riege, R. A. London, and A. Szoke, Dynamics of biological molecules irradiated by short x-ray pulses, *Phys. Rev. E* **69**, 051906 (2004).

[30] N. Medvedev and B. Ziaja, Multistep transition of diamond to warm dense matter state revealed by femtosecond x-ray diffraction, *Sci. Rep.* **8**, 5284 (2018).

[31] S. P. Hau-Riege, X-ray atomic scattering factors of low- Z ions with a core hole, *Phys. Rev. A* **76**, 042511 (2007).

[32] S.-K. Son, L. Young, and R. Santra, Impact of hollow-atom formation on coherent x-ray scattering at high intensity, *Phys. Rev. A* **83**, 033402 (2011).

[33] H. M. Quiney and K. A. Nugent, Biomolecular imaging and electronic damage using x-ray free-electron lasers, *Nat. Physics* **7**, 142 (2011).

[34] S.-K. Son, H. N. Chapman, and R. Santra, Multiwavelength anomalous diffraction at high x-ray intensity, *Phys. Rev. Lett.* **107**, 218102 (2011).

[35] S.-K. Son, H. N. Chapman, and R. Santra, Determination of multiwavelength anomalous diffraction coefficients at high x-ray intensity, *J. Phys. B* **46**, 164015 (2013).

[36] K. R. Ferguson, M. Bucher, T. Gorkhov, S. Boutet, H. Fukuzawa, J. E. Koglin, Y. Kumagai, A. Lutman, A. Marinelli, M. Messerschmidt, K. Nagaya, J. Turner, K. Ueda, G. J. Williams, P. H. Bucksbaum, and C. Bostedt, Transient lattice contraction in the solid-to-plasma transition, *Science Advances* **2**, e1500837 (2016).

[37] K. Nass, A. Gorel, M. M. Abdullah, A. V. Martin, M. Kloos, A. Marinelli, A. Aquila, T. R. M. Barends, F.-J. Decker, R. Bruce Doak, L. Foucar, E. Hartmann, M. Hilpert, M. S. Hunter, Z. Jurek, J. E. Koglin, A. Kozlov, A. A. Lutman, G. N. Kovacs, C. M. Roome, R. L. Shoeman, R. Santra, H. M. Quiney, B. Ziaja, S. Boutet, and I. Schlichting, Structural dynamics in proteins induced by and probed with x-ray free-electron laser pulses, *Nat. Commun.* **11**, 1814 (2020).

[38] T. Ishikawa, H. Aoyagi, T. Asaka, Y. Asano, N. Azumi, T. Bizen, H. Ego, K. Fukami, T. Fukui, Y. Furukawa, S. Goto, H. Hanaki, T. Hara, T. Hasegawa, T. Hattori, A. Higashiyama, T. Hiroto, N. Hosoda, M. Ishii, T. Inagaki, Y. Inubushi, T. Itoga, Y. Joti, M. Kago, T. Kameshima, H. Kimura, Y. Kiriha, A. Kiyomichi, T. Kobayashi, C. Kondo, T. Kudo, H. Maesaka, X. M. Maréchal, T. Masuda, S. Matsubara, T. Matsumoto, T. Matsushita, S. Matsui, M. Nagasono, N. Nariyama, H. Ohashi, T. Ohata, T. Ohshima, S. Ono, Y. Otake, C. Saji, T. Sakurai, T. Sato, K. Sawada, T. Seike, K. Shirasawa, T. Sugimoto, S. Suzuki, S. Takahashi, H. Takebe, K. Takeshita, K. Tamasaku, H. Tanaka, R. Tanaka, T. Tanaka, T. Togashi, K. Togawa, A. Tokuhisa, H. Tomizawa, K. Tono, S. Wu, M. Yabashi, M. Yamaga, A. Yamashita, K. Yanagida, C. Zhang, T. Shintake, H. Kitamura, and N. Kumagai, A compact x-ray free-electron laser emitting in the sub-ångström region, *Nat. Photonics* **6**, 540 (2012).

[39] Y. Inubushi, I. Inoue, J. Kim, A. Nishihara, S. Matsuyama, H. Yumoto, T. Koyama, K. Tono, H. Ohashi, K. Yamauchi, and M. Yabashi, Measurement of the x-ray spectrum of a free electron laser with a wide-range high-resolution single-shot spectrometer, *Appl. Sci.* **7** (2017).

[40] I. Inoue, T. Hara, Y. Inubushi, K. Tono, T. Inagaki, T. Katayama, Y. Amemiya, H. Tanaka, and M. Yabashi, X-ray hanbury brown-twiss interferometry for determination of ultrashort electron-bunch duration, *Phys. Rev. Accel. Beams* **21**, 080704 (2018).

[41] I. Inoue, K. Tamasaku, T. Osaka, Y. Inubushi, and M. Yabashi, Determination of X-ray pulse duration via intensity correlation measurements of X-ray fluorescence, *J. Synchrotron Radiat.* **26**, 2050 (2019).

[42] M. Yabashi, H. Tanaka, and T. Ishikawa, Overview of the SACLÀ facility, *J. Synchrotron Radiat.* **22**, 477 (2015).

[43] K. Tono, T. Togashi, Y. Inubushi, T. Katayama, S. Owada, T. Yabuuchi, A. Kon, I. Inoue, T. Osaka, H. Yumoto, T. Koyama, H. Ohashi, and M. Yabashi, Overview of optics, photon diagnostics and experimental instruments at SACLÀ: development, operation and scientific applications, in *SPIE Advances in X-ray Free-Electron Lasers Instrumentation IV*, Vol. 10237, edited by T. Tschenetscher and L. Patthey (International Society for Optics and Photonics, 2017) pp. 1 – 10.

[44] T. Kameshima, S. Ono, T. Kudo, K. Ozaki, Y. Kiriha, K. Kobayashi, Y. Inubushi, M. Yabashi, T. Horigome, A. Holland, K. Holland, D. Burt, H. Murao, and T. Hattori, Development of an x-ray pixel detector with multiport charge-coupled device for x-ray free-electron laser experiments, *Rev. Sci. Instruments* **85**, 033110 (2014).

[45] K. Tono, T. Togashi, Y. Inubushi, T. Sato, T. Katayama, K. Ogawa, H. Ohashi, H. Kimura, S. Takahashi, K. Takeshita, H. Tomizawa, S. Goto, T. Ishikawa, and M. Yabashi, Beamline, experimental stations and photon beam diagnostics for the hard x-ray free electron laser of SACLÀ, *New J. Phys.* **15**, 083035 (2013).

[46] N. Medvedev, M. Kopecky, J. Chalupsky, and L. Juha, Femtosecond x-ray diffraction can discern nonthermal from thermal melting, *Phys. Rev. B* **99**, 100303 (2019).

[47] A. Barty, C. Caleman, A. Aquila, N. Timneanu, L. Lomb, T. A. White, J. Andreasson, D. Arnlund, S. Bajt, T. R. M. Barends, M. Barthelmess, M. J. Bogan, C. Bostedt, J. D. Bozek, R. Coffee, N. Coppola, J. Davidsson, D. P. DePonte, R. B. Doak, T. Ekeberg, V. Elser, S. W. Epp, B. Erk, H. Fleckenstein, L. Foucar, P. Fromme, H. Graafsma, L. Gumprecht, J. Hajdu, C. Y. Hampton, R. Hartmann, A. Hartmann, G. Hauser, H. Hirsemann, P. Holl, M. S. Hunter, L. Johansson, S. Kassemeyer, N. Kimmel, R. A. Kirian, M. Liang, F. R. N. C. Maia, E. Malmerberg, S. Marchesini, A. V. Martin, K. Nass, R. Neutze, C. Reich, D. Rolles, B. Rudek, A. Rudenko, H. Scott, I. Schlichting, J. Schulz, M. M. Seibert, R. L. Shoeman, R. G. Sierra, H. Soltau, J. C. H. Spence, F. Stellato, S. Stern, L. Strüder, J. Ullrich, X. Wang, G. Weidenspointner, U. Weierstall, C. B. Wunderer, and H. N. Chapman, Self-terminating diffraction gates femtosecond x-ray nanocrystallography measurements, *Nat. Photonics* **6**, 35 (2012).

[48] Z. Jurek, S.-K. Son, B. Ziaja, and R. Santra, *XMDYN* and *XATOM*: versatile simulation tools for quantitative modeling of X-ray free-electron laser induced dynamics of matter, *J. App. Crystallogr.* **49**, 1048 (2016).

[49] B. F. Murphy, T. Osipov, Z. Jurek, L. Fang, S. K. Son, M. Mucke, J. H. D. Eland, V. Zhaunerchyk, R. Feifel, L. Avaldi, P. Bolognesi, C. Bostedt, J. D. Bozek, J. Grilj, M. Guehr, L. J. Frasinski, J. Glownia, D. T. Ha, K. Hoffmann, E. Kukk, B. K. McFarland, C. Miron, E. Sistrunk, R. J. Squibb, K. Ueda, R. Santra, and N. Berrah, Femtosecond x-ray-induced explosion of c60 at extreme intensity, *Nat. Commun.* **5**, 4281 (2014).

[50] I. Inoue, Y. Inubushi, T. Osaka, J. Yamada,

K. Tamasaku, H. Yoneda, and M. Yabashi, Shortening x-ray pulse duration via saturable absorption, *Phys. Rev. Lett.* **127**, 163903 (2021).

[51] Z. Huang and R. D. Ruth, Fully coherent x-ray pulses from a regenerative-amplifier free-electron laser, *Phys. Rev. Lett.* **96**, 144801 (2006).

[52] K.-J. Kim, Y. Shvyd'ko, and S. Reiche, A proposal for an x-ray free-electron laser oscillator with an energy-recovery linac, *Phys. Rev. Lett.* **100**, 244802 (2008).

[53] W. Lotz, Electron-impact ionization cross-sections and ionization rate coefficients for atoms and ions from hydrogen to calcium, *Zeitschrift für Physik* **216**, 241 (1968).